Sheffield Hallam University

Theoretical and Practical Implications Derived From the Formulation of the Theory of Critical Distances

CICERO, Sergio <http://orcid.org/0000-0002-3950-6071>, TAYLOR, David <http://orcid.org/0000-0002-5470-2062> and SUSMEL, Luca <http://orcid.org/0000-0001-7753-9176>

Available from Sheffield Hallam University Research Archive (SHURA) at:

https://shura.shu.ac.uk/37252/

This document is the Published Version [VoR]

Citation:

CICERO, Sergio, TAYLOR, David and SUSMEL, Luca (2026). Theoretical and Practical Implications Derived From the Formulation of the Theory of Critical Distances. Fatigue & Fracture of Engineering Materials & Structures, 49 (7), 2610-2618. [Article]

Copyright and re-use policy

See http://shura.shu.ac.uk/information.html

Sheffield Hallam University Research Archive
http://shura.shu.ac.uk

Check for updates

Fatigue & Fracture of Engineering Materials & Structures

WILEY

FFEMS Fatigue & Fracture of Engineering Materials & Structures

ORIGINAL ARTICLE OPEN ACCESS

Theoretical and Practical Implications Derived From the Formulation of the Theory of Critical Distances

Sergio Cicero[1] | David Taylor[2,3] | Luca Susmel[4]

[1]LADICIM, Universidad de Cantabria, ETS Ingenieros de Caminos, Santander, Spain | [2]Trinity Centre for Biomedical Engineering, Trinity Biomedical Sciences Institute, Trinity College Dublin, Dublin, Ireland | [3]Department of Mechanical, Manufacturing and Biomedical Engineering, School of Engineering, Trinity College Dublin, Dublin, Ireland | [4]School of Engineering and Built Environment, Sheffield Hallam University, Sheffield, UK

Correspondence: Sergio Cicero (sergio.cicero@unican.es)

Received: 29 January 2026 | **Revised:** 17 March 2026 | **Accepted:** 25 March 2026

Keywords: line method | notch | point method | theory of critical distances

ABSTRACT

The Theory of Critical Distances comprises several methodologies that allow fracture, fatigue, and stress corrosion cracking phenomena to be analyzed. Such methodologies are usually referred to as the Point Method (PM), the Line Method (LM), the Area Method (AM), and the Volume Method (VM). All of them provide analyses where the corresponding material resistance (e.g., fracture toughness, fatigue threshold, and stress corrosion cracking threshold) is used together with an additional material parameter with length units (the critical distance, L). Moreover, the accuracy of these four approaches is very similar, but the PM and the LM have a much simpler application. When dealing with fracture processes, the TCD allows fracture conditions for structural materials in the presence of notch-type defects to be established, and simple formulas for estimating the apparent fracture toughness (i.e., the fracture resistance in the presence of notches) to be obtained. This paper provides a number basic reasonings related to both the PM and/or the LM formulations that allow different straightforward conclusions to be derived, with significant theoretical and practical implications. Real cases with experimental results are also included, exemplifying what is discussed in the theoretical analysis.

1 | Introduction

The presence of notches in structural parts is a very common phenomenon. Actually, there are frequent situations where the existing defects endangering the structural integrity of the corresponding component are not crack-like defects (i.e., infinitely sharp defects). Examples are mechanical damage, corrosion defects, pores or fabrication defects (among others), and drilled holes and slots. These defects, which are generally referred to as notches, have a finite radius on their tip that diminishes the severity of the stress field and, as shown in [1–4], can also generate modifications in the fracture micromechanisms.

Regarding the assessment of structural components containing notches, the simplest approach consists in considering that they behave like crack-like defects and, consequently, applying conventional fracture mechanics approaches. This, however, is generally an overconservative assumption, provided that there is vast scientific and technical evidence in literature (e.g., [1–8]) revealing how, in the presence of notches, materials develop a fracture resistance that is larger (to different extents, depending on the specific material being analyzed) than the fracture toughness (K_{mat}) developed by such materials in the presence of crack-like defects. This higher fracture resistance, usually referred to as the apparent fracture toughness K^{N}_{mat}), may have direct significant consequences on important variables related to the structural integrity, such as the resulting load-bearing capacity or the maximum allowed defect size. Similar observations can be made regarding subcritical cracking processes, such as fatigue and stress corrosion cracking.

This is an open access article under the terms of the Creative Commons Attribution License, which permits use, distribution and reproduction in any medium, provided the original work is properly cited.

© 2026 The Author(s). *Fatigue & Fracture of Engineering Materials & Structures* published by John Wiley & Sons Ltd.

Consequently, the analysis of cracking processes in materials containing notches requires the definition of particularized assessment tools (e.g., [1, 5–9]). In this sense, there have been different proposals to address the specific nature of notch-type defects, such as notch fracture mechanics approaches [10], the Average Strain Energy Density Criterion [11] or the Theory of Critical Distances (TCD) [1]. The latter stands out for its capacity to provide assessment solutions for a wide range of cracking processes (i.e., fracture, fatigue processes, and stress corrosion cracking) and has been widely validated by different authors (e.g., [1]). Regarding fracture assessments, and knowing that there are analogous formulations for other cracking processes such as fatigue [1] or stress corrosion cracking [12], the TCD is essentially a set of different methodologies (e.g., Point Method, Line Method, Area Method and Volume Method) [1] that make use of a material length parameter (referred to as the critical distance, L), together with the material fracture toughness (K_{mat}), to establish the critical fracture conditions. L, which measures the material sensitivity to notch effect, follows Equation (1):

$$L = \frac{1}{\pi}\left(\frac{K_{mat}}{\sigma_0}\right)^2 \tag{1}$$

σ_0 being the material inherent strength. In materials with linear-elastic behavior at both the micro- and the macroscales (e.g., fracture of ceramics), σ_0 equates to the material tensile strength σ_u. However, any nonlinearity in the material behavior implies that σ_0 deviates from σ_u, requiring a specific calibration process. For fatigue processes, L follows an analogous expression, with K_{mat} being substituted by ΔK_{th} and σ_0 being replaced by the fatigue limit ($\Delta\sigma_0$).

The simplest approach, the Point Method (PM), states that fracture occurs when the stress at a distance of L/2 from the crack tip equals the material inherent strength:

$$\sigma\left(\frac{L}{2}\right) = \sigma_0 \tag{2}$$

Analogously, the Line Method (LM) states that fracture occurs when the average stress along a distance equal to 2L (measured from the notch tip) equals σ_0:

$$\frac{1}{2L}\int_0^{2L} \sigma(r)dr = \sigma_0 \tag{3}$$

In the case of slender U-notches, whose stress field may be defined by the Creager–Paris stress distribution at the notch tip (Equation (4)) [13], the combination of the Line Method and such stress distribution leads to Equation (5) [1], which provides the apparent fracture toughness (K^N_{mat}) of the material in the presence of a notch with radius ρ. In Equation (4), K_I is the mode I stress intensity factor, ρ is the notch radius, and r is the distance existing from the notch tip to the point being assessed.

$$\sigma(r) = \frac{K_I}{\sqrt{\pi}}\frac{2(r+\rho)}{(2r+\rho)^{3/2}} \tag{4}$$

$$K^N_{mat} = K_{mat}\sqrt{1+\frac{\rho}{4L}} \tag{5}$$

Based on these very simple formulations, this paper provides several theoretical reasonings with theoretical and practical implications that may be helpful for those using the TCD to analyze notch-type defects. Real cases are also included, showing how theoretical analyses relate to the actual behavior of structural materials in the presence of defects. The analyses are mainly focused on fracture processes, with some comments related to fatigue phenomena, although similar reasonings could be derived for the abovementioned subcritical processes.

2 | Theoretical Reasonings and Implications

2.1 | Reasoning 1

Figure 1 represents the critical stress field of two materials, A and B, with the same value of critical distance ($L_A = L_B$) and where it is assumed that σ_{uB} is higher than σ_{uA}. Providing the stress response is linear, the ratio of critical loads is the same as the ratio of tensile strengths.

The simple application of the PM reveals that the material providing the larger load-bearing capacity is the one with the highest tensile strength.

Implication 1a. Assuming linear-elastic behavior, two materials with identical L (same sensitivity to notch effect) will have, for a given notch radius, critical loads (P_{crit}) ratio equal to the tensile strengths ratio (or equal to the inherent strengths ratio, for nonfully linear-elastic situations).

$$P_{crit.B} = P_{crit.A}\left(\frac{\sigma_{uB}}{\sigma_{uA}}\right) \tag{6}$$

Implication 1b. In the same case of identical L, if σ_{uB} is higher than σ_{uA}, $K_{mat,B}$ is necessarily higher than $K_{mat,A}$ (see Equation (1)).

Implication 1c. Again, if L is identical, the toughness to strength ratio is also identical (see Equation (9)). Thus, the

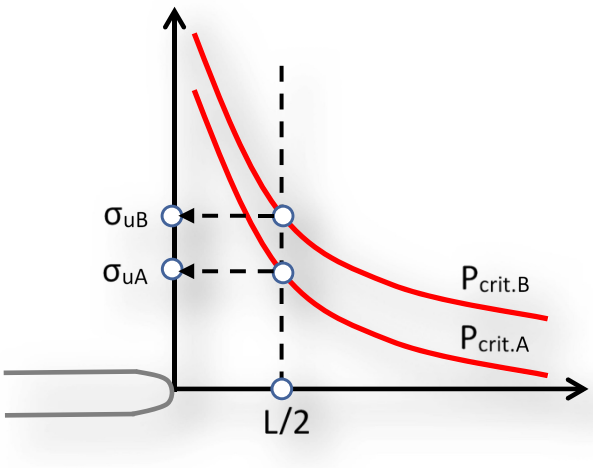

FIGURE 1 | Schematic of the critical condition in two materials, A and B, with the same critical distance (L) and following the Point Method. [Colour figure can be viewed at wileyonlinelibrary.com]

14602695, 2026, 7, Downloaded from https://onlinelibrary.wiley.com/doi/10.1111/ffe.70282 by Sheffield Hallam University, Wiley Online Library on [08/06/2026]. See the Terms and Conditions (https://onlinelibrary.wiley.com/terms-and-conditions) on Wiley Online Library for rules of use; OA articles are governed by the applicable Creative Commons License

critical load is not only proportional to the tensile strength but it is also proportional to the fracture toughness.

$$L_A = \frac{1}{\pi}\left(\frac{K_{mat,A}}{\sigma_{uA}}\right)^2 \tag{7}$$

$$L_B = \frac{1}{\pi}\left(\frac{K_{mat,B}}{\sigma_{uB}}\right)^2 \tag{8}$$

$$L_A = L_B \rightarrow \frac{K_{mat,A}}{\sigma_{uA}} = \frac{K_{mat,B}}{\sigma_{uB}} \tag{9}$$

Cicero et al. [14, 15] characterized the fracture behavior of additively manufactured PLA and graphene-reinforced PLA (PLA-Gr, 1 wt.%). The fracture characterization was performed on U-notched SENB specimens printed with different raster orientations (0/90, 30/−60, 45/−45) and containing notch radii from 0 mm (crack-like defects) up to 2.0 mm, as shown in Figure 2. Two of the resulting materials, PLA 30/−60 and PLA-Gr 0/90, have the same value of L (0.67 mm), derived from the best fit of Equation (5) to a number of experimental results. Additionally, σ_0 resulted in 125.5 and 122.2 MPa, respectively, when applying the LM, and 171.2 and 160.2 MPa when applying the PM. Thus, the ratio between the inherent strengths of these two materials may be reasonably established between 1.027 and 1.068. Looking at the average fracture loads in both materials for the different analyzed notch radii, they result in 231.3 and 192.8 N for notch radius 0.25 mm; 242.1 and 201.0 N for notch radius 0.5 mm; 262.8 and 217.0 N for notch radius 1.0 mm; and 209.6 and 189.0 N for notch radius 2.0 mm, leading to critical load ratios of 1.199, 1.204, 1.210, and 1.108, respectively, which are reasonably similar to the inherent strengths ratio and, in any case, reveal how, for two materials with the same L, the one with higher inherent strength sustains higher critical loads.

Moreover, it can be observed how, as stated in Implication 1b, K_{mat} is also (slightly) higher in PLA 30/−60 material.

Another interesting example, related to fatigue analysis, may be found in [1] (section 12.4). The author presents a case study consisting of a large cast-iron structure that was suffering fatigue cracking from a sharp, right-angle corner. Different geometrical configurations were analyzed, leading to different R ($\sigma_{min}/\sigma_{max}$) ratios. For the different configurations, L remained fairly constant (around 3.8 mm), but one of the configurations, associated with a reduction of the maximum load on the component, was able to prevent further fatigue failures. The authors show how for this particular configuration (and R ratio), L is similar to that in other cases, but this constant L is achieved through significantly higher values of both ΔK_{th} and $\Delta\sigma_0$.

2.2 | Reasoning 2

Now, let us consider two materials with the same tensile strength (σ_u) or, more generally, the same inherent strength (σ_0). The stress profiles at fracture, for the same component geometry and for linear-elastic conditions, are shown in Figure 3, where (following the PM) it is evident that the material with larger L (lower sensitivity to notch effect) will have a higher critical load.

Implication 2a. Under linear-elastic conditions, for two materials having the same tensile strength (or, more generally, the same σ_0 in nonfully linear conditions), the material with larger L will sustain higher critical loads.

Implication 2b. If σ_u is the same for two materials, the material with larger L will necessarily have a larger fracture toughness (K_{mat}) (see Equation (1)).

Looking again to the same experimental program mentioned above [14, 15], there are two materials with very similar σ_0 and rather different L values: PLA 30/−60, with (as mentioned before) σ_0 and L values of 125.5 MPa and 0.67 mm, and; PLA-Gr 45/−45, with σ_0 and L values of 124.7 MPa and 1.06 mm.

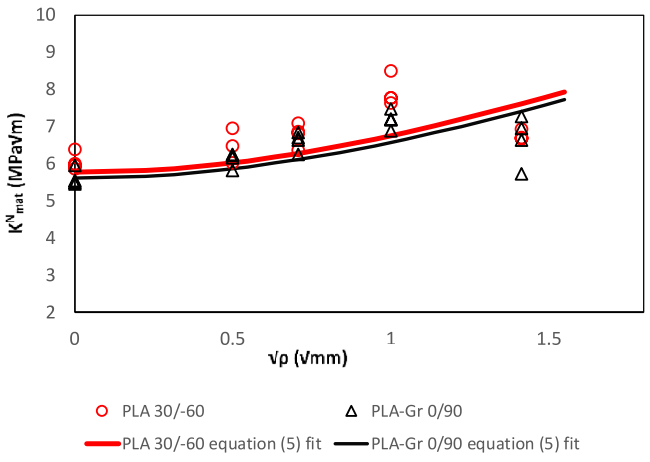

FIGURE 2 | Fracture results on PLA 30/−60 and PLA-Gr 0/90 additively manufactured materials, generating the same value of L (0.67 mm). [Colour figure can be viewed at wileyonlinelibrary.com]

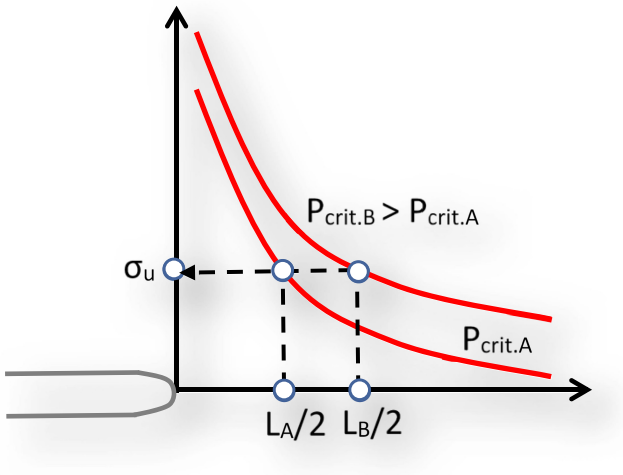

FIGURE 3 | Schematic of the critical condition in two materials, A and B, with the same tensile strength (σ_u) and following the Point Method. [Colour figure can be viewed at wileyonlinelibrary.com]

14602695, 2026, 7, Downloaded from https://onlinelibrary.wiley.com/doi/10.1111/ffe.70282 by Sheffield Hallam University, Wiley Online Library on [08/06/2026]. See the Terms and Conditions (https://onlinelibrary.wiley.com/terms-and-conditions) on Wiley Online Library for rules of use; OA articles are governed by the applicable Creative Commons License

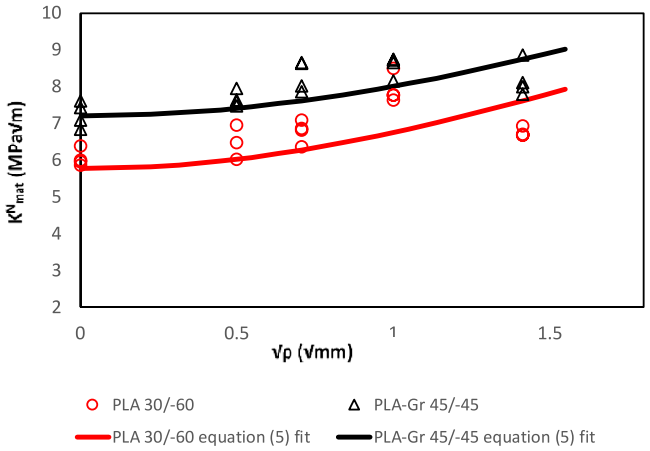

FIGURE 4 | Fracture results on PLA 30/−60 and PLA-Gr 45/−45 additively manufactured materials, both having similar σ_0 (≈125 MPa). [Colour figure can be viewed at wileyonlinelibrary.com]

Figure 4 shows the results obtained in the fracture characterization tests, together with the corresponding fittings. The corresponding average fracture loads in both materials (PLA 30/−60 and PLA-Gr 45/−45) for the different analyzed notch radii are 231.3 and 251.9 N for notch radius 0.25 mm; 242.1 and 267.5 N for notch radius 0.5 mm; 262.8 and 272.6 N for notch radius 1.0 mm; and 209.6 and 216.6.0 N for notch radius 2.0 mm. Thus, indeed, the material with higher L always sustain higher critical loads.

Finally, as stated in Implication 2b, the material with larger L (PLA-Gr 45/−45) has a higher K_{mat} (and higher K^N_{mat} within the range of notch radii being analyzed).

2.3 | Reasoning 3

Figure 5 reveals what can be expected from two materials with two different values of L and σ_u. The schematic reveals that if $L_B < L_A$ and $\sigma_{uB} < \sigma_{uA}$ (Zone 1 in the figure), Material A will always sustain higher critical loads.

Let us assume two materials with critical distances L_A and L_B, respectively, with L_A being larger than L_B and following Equation (10):

$$L_B = \frac{1}{\pi}\left(\frac{K_{mat,B}}{\sigma_{uB}}\right)^2 = c \cdot L_A = c \cdot \frac{1}{\pi}\left(\frac{K_{mat,A}}{\sigma_{uA}}\right)^2 \qquad c < 1 \quad (10)$$

c being the ratio between the two critical distances (i.e., L_B/L_A). The terms in Equation (10) can be grouped, leading to

$$\sigma_{uB} = \sigma_{uA}\left(\frac{K_{mat,B}}{K_{mat,A}}\right)\frac{1}{\sqrt{c}} \quad (11)$$

As shown above, and provided $L_B < L_A$, the condition ensuring that $P_{crit,B}$ is always lower than $P_{crit,A}$ is that $\sigma_{uB} < \sigma_{uA}$:

$$\sigma_{uB} = \sigma_{uA}\left(\frac{K_{mat,B}}{K_{mat,A}}\right)\frac{1}{\sqrt{c}} < \sigma_{uA} \quad (12)$$

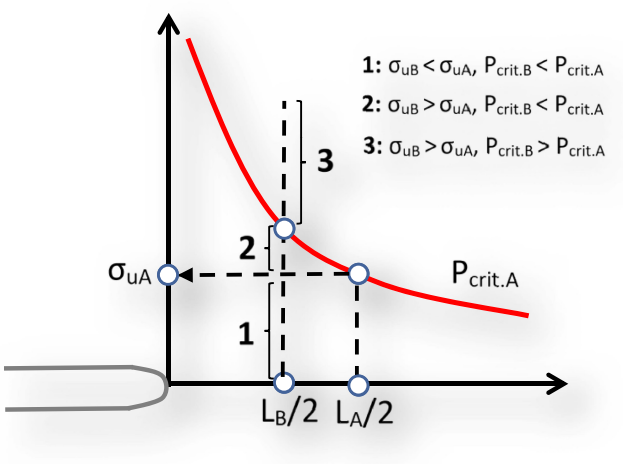

FIGURE 5 | Schematic of the critical condition in Material A (Point Method), and possible critical conditions in Material B for different values of σ_{uB}. [Colour figure can be viewed at wileyonlinelibrary.com]

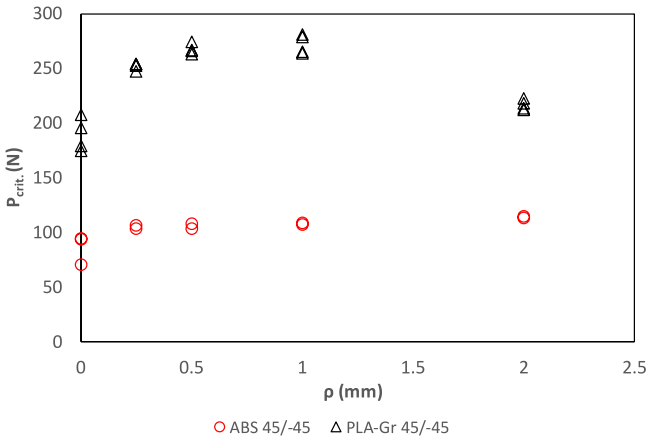

FIGURE 6 | Critical loads on ABS 45/−45 and PLA-Gr 45/−45 additively manufactured materials, the former having lower L and σ_0 values. [Colour figure can be viewed at wileyonlinelibrary.com]

This leads to

$$K_{mat,B} < \sqrt{c} \cdot K_{mat,A} = \sqrt{\frac{L_B}{L_A}} \cdot K_{mat,A} \quad (13)$$

Higher values of σ_{uB} may also lead to lower values of $P_{crit,B}$ compared to $P_{crit,A}$ (see Zone II in Figure 5), but this would depend on the shape of the stress profile and, thus, on the particular geometry of the defect and the component being analyzed.

Implication 3. Given two materials, A and B, with $L_A > L_B$, $P_{crit.A}$ will always be higher than $P_{crit.B}$ if $\sigma_{uA} > \sigma_{uB}$ or, alternatively, if $K_{mat,A} > K_{mat,B}$ (L_A/L_B).

The same PLA-Gr 45/−45 [14, 15] can now be compared with additively manufactured ABS 45/−45 [16], which was tested following a similar experimental program and using SENB specimens with the same geometry (so that the critical loads can be directly compared). PLA-Gr 45/−45 has L and σ_0 values of 1.06 and 124.7 mm, respectively, whereas such properties

14602695, 2026, 7, Downloaded from https://onlinelibrary.wiley.com/doi/10.1111/ffe.70282 by Sheffield Hallam University, Wiley Online Library on [08/06/2026]. See the Terms and Conditions (https://onlinelibrary.wiley.com/terms-and-conditions) on Wiley Online Library for rules of use; OA articles are governed by the applicable Creative Commons License

in ABS 45/−45 are 0.55 mm and 99.1 MPa. Accordingly, given that both values are higher in PLA-Gr 45/−45, this material should provide higher critical loads. This is verified in Figure 6, where it can be observed how the critical loads of PLA-Gr 45/−45 are significantly higher than those generated by ABS 45/−45.

2.4 | Reasoning 4

Figure 7 shows the schematic of two materials with different values of σ_u (or σ_0) and L that, for the particular notch radius being analyzed, generate the same critical load (P_{crit}) when applying the Point Method. This situation is particular for such notch radius, but for any other notch radius the two materials would provide different critical loads (P'_{crit}), as described by the dotted lines shown in the figure, which corresponds to a larger notch radius (less demanding stress field) and where Material B is able to sustain a higher critical load.

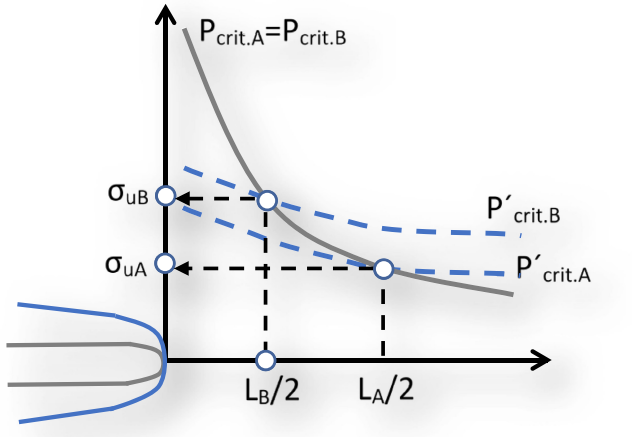

FIGURE 7 | Stress fields and critical conditions for two materials, A and B, with different values of σ_0 and L and for two different notch radii. [Colour figure can be viewed at wileyonlinelibrary.com]

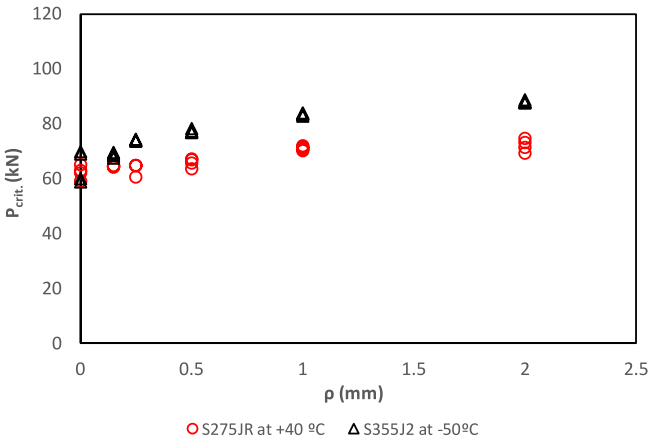

FIGURE 8 | Critical loads for steels S275JR (+40°C) and S355J2 (−50°C), showing similar values under cracked conditions, with the latter exhibiting a lower L. [Colour figure can be viewed at wileyonlinelibrary.com]

Implication 4. If two materials have the same critical load for a given notch radius, if the radius is increased, the material with lower L (B in Figure 7) will sustain higher critical loads ($P'_{crit.B} > P'_{crit.A}$), whereas if the radius is reduced it would be the material with larger L that would be able to sustain higher loads.

This can be exemplified by the results obtained in [17] on ferritic steels (see Figure 8). In cracked conditions ($\rho = 0$ mm), steels S275JR at 40°C and S355J2 at −50°C provide very similar (average) critical loads on 25-mm thick CT specimens: 62.3 and 64.4 kN, respectively. However, when the notch radius is increased up to 2.0 mm, the corresponding critical loads are 72.2 and 88.0 kN, respectively. Looking at their critical distance values, indeed, steel S355J2 has a significantly lower L (0.0778 mm) than steel S275JR (0.1697 mm). Therefore, the results satisfy Implication 4, even in cases such as the one shown, where the conditions deviate significantly from linear elasticity.

2.5 | Reasoning 5

For U-notches, whose stress field for sufficiently slender defects may be defined by the Creager–Paris stress distribution at the notch tip (Equation (4)), the apparent fracture toughness (K^N_{mat}) of the material in the presence of a notch with radius ρ may be quantified by Equation (5). In such equation, the term in the square root is the resulting notch effect correction.

Now, for two materials, A and B, and for a particular notch radius, the corresponding predictions of K^N_{mat} are given by Equations (14) and (15). If, again, the two materials have the same sensitivity to notch effect (i.e., $L_A = L_B$), the notch correction is also the same, and, additionally, Equation (16) provides the relation between apparent fracture toughness values and fracture toughness values.

$$K^N_{mat,\ A} = K_{mat,A}\sqrt{1+\frac{\rho}{4L_A}} \tag{14}$$

$$K^N_{mat,\ B} = K_{mat,B}\sqrt{1+\frac{\rho}{4L_B}} \tag{15}$$

$$\frac{K^N_{mat,\ A}}{K^N_{mat,\ B}} = \frac{K_{mat,A}}{K_{mat,B}} \tag{16}$$

Implication 5a. Under linear-elastic conditions, two materials with the same critical distance have the same notch effect (and correction) for a given notch radius.

Implication 5b. Accordingly, the ratio of apparent fracture toughness values is equal to the ratio of fracture toughness values (Equation (16)) for any notch radius being considered.

These two implications may be clearly observed in Figure 2.

2.6 | Reasoning 6

Considering two materials, A and B, with the same fracture toughness in cracked conditions (K_{mat}), Equation (5) allows the

14602695, 2026, 7, Downloaded from https://onlinelibrary.wiley.com/doi/10.1111/ffe.70282 by Sheffield Hallam University, Wiley Online Library on [08/06/2026]. See the Terms and Conditions (https://onlinelibrary.wiley.com/terms-and-conditions) on Wiley Online Library for rules of use; OA articles are governed by the applicable Creative Commons License

evolution of the apparent fracture toughness with the notch radius to be represented. The schematic shown in Figure 5 reveals how such apparent fracture toughness is higher, for any notch radius (ρ), for the material with lower critical distance (i.e., higher sensitivity to notch effect). Moreover, those materials with very high critical distance would have a nearly flat curve (see Material C in Figure 9) for a wide range of notch radii, with a very similar resistance in cracked and notched conditions (regardless of the notch radius dimension).

Implication 6a. If two materials, A and B, have the same fracture toughness (K_{mat}), the material with lower L will always develop larger fracture resistance in notched conditions for any notch radius being considered (they are equal just at cracked conditions).

Implication 6b. Following Equation (5), it is straightforward to check that for notch radii below the material critical distance, the resulting increase in the material fracture resistance (i.e., the difference between apparent fracture toughness and the fracture toughness) is very limited. Actually, for $\rho/L = 1$, such increase is limited to 11%.

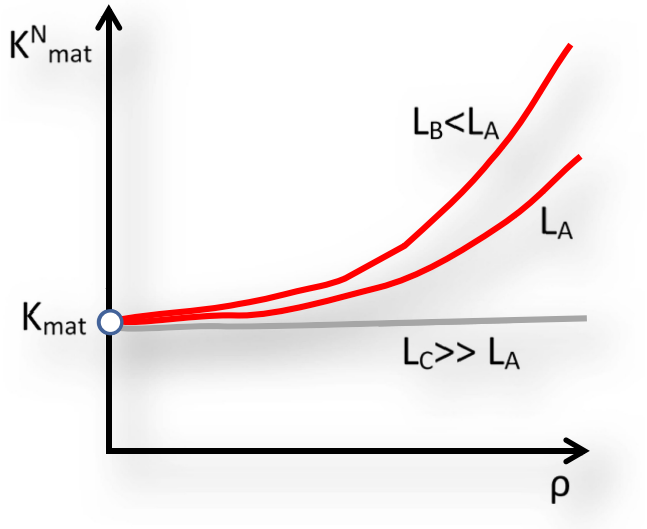

FIGURE 9 | Evolution of apparent fracture toughness (K^N_{mat}) in materials with same fracture toughness (K_{mat}) and different values of critical distance (L). [Colour figure can be viewed at wileyonlinelibrary.com]

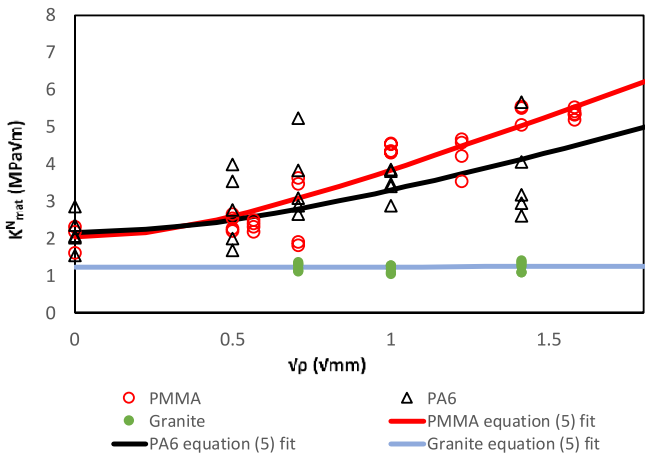

FIGURE 10 | Evolution of K^N_{mat} in PMMA and PA6, both having similar K_{mat} and different values of L, and in Granite (material with very high L). [Colour figure can be viewed at wileyonlinelibrary.com]

Figure 10 shows experimental results on PMMA [2] and PA6 [18]. They both present very similar values of K_{mat} (2.04 MPam$^{1/2}$ and 2.17 MPam$^{1/2}$). However, L is 0.098 mm for PMMA and 0.190 mm for PA6, which makes that, beyond the experimental scatter, PMMA provides higher (average) values of K^N_{mat} when the notch radius increases. The figure also shows the evolution of K^N_{mat} in granite [19], a material with very high L (46.6 mm) and, thus, presenting a negligible evolution of K^N_{mat} for the notch radii being analyzed.

2.7 | Reasoning 7

Given two materials, A and B, with different values of fracture toughness in cracked conditions ($K_{mat,B} > K_{mat,A}$), Equation (17) allows calculating the notch radius (ρ^*) above which the apparent fracture toughness developed by Material A is higher than that developed by Material B (see Figure 11). This necessarily requires L_A to be lower than L_B, with ρ^* being given by Equation (18).

$$K_{mat,A}\sqrt{1+\frac{\rho^*}{4L_A}} = K_{mat,B}\sqrt{1+\frac{\rho^*}{4L_B}} \tag{17}$$

$$\rho^* = \frac{K^2_{mat,B} - K^2_{mat,A}}{\frac{K^2_{mat,A}}{4L_A} - \frac{K^2_{mat,B}}{4L_B}} \tag{18}$$

Equation (18) can be directly applied in engineering practice to determine, based on notch geometry (i.e., notch radius) and the mechanical properties of different materials, which

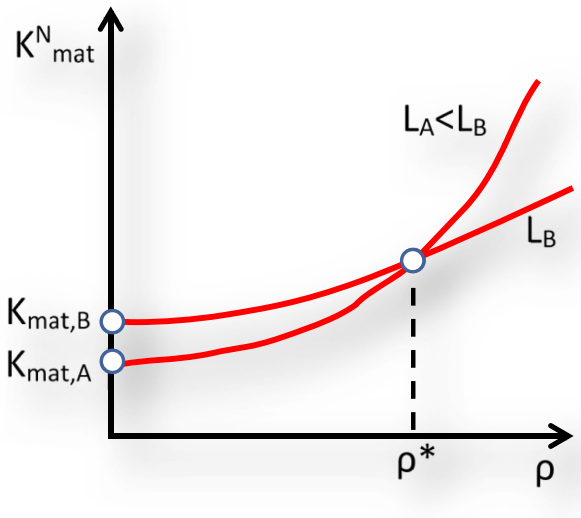

FIGURE 11 | Evolution of apparent fracture toughness (K^N_{mat}) in materials with different fracture toughness (K_{mat}) and critical distance and definition of the notch radius (ρ^*) at which their apparent fracture toughness is equal. [Colour figure can be viewed at wileyonlinelibrary.com]

14602695, 2026, 7, Downloaded from https://onlinelibrary.wiley.com/doi/10.1111/ffe.70282 by Sheffield Hallam University, Wiley Online Library on [08/06/2026]. See the Terms and Conditions (https://onlinelibrary.wiley.com/terms-and-conditions) on Wiley Online Library for rules of use; OA articles are governed by the applicable Creative Commons License

material is most suitable from a structural integrity standpoint. Alternatively, Equation (18) can be used to determine the range of notch radii for which a given material provides greater fracture resistance than others.

Implication 7a. Looking at Equation (18), where it has been assumed that the numerator is positive, in order to obtain a ρ^* value with physical meaning (i.e., $\rho^* > 0$), the denominator has to be also positive. This provides the required condition of L_A in order Material A to be able to develop larger apparent fracture toughness than Material B for notch radii values beyond ρ^*.

$$L_A < \left(\frac{K_{mat,A}}{K_{mat,B}}\right)^2 L_B \tag{19}$$

Implication 7b. If L_A is equal to L_B, there is no ρ^* and, even more, the ratio of apparent fracture toughness values is equal to the ratio of fracture toughness values for any notch radius being considered (as mentioned in Section 2.5).

$$\frac{K^N_{mat,A}}{K^N_{mat,B}} = \frac{K_{mat,A}\sqrt{1+\frac{\rho^*}{4L_A}}}{K_{mat,B}\sqrt{1+\frac{\rho^*}{4L_B}}} = \frac{K_{mat,A}}{K_{mat,B}} \tag{20}$$

One example of this situation may be found in [20], which analyzes the fracture behavior of U-notched additively manufactured carbon fiber reinforced (10 wt.%) ASA. When comparing the fracture behavior in specimens printed with different raster orientations (see Figure 12), the results for 0/90 and 45/−45 materials are very interesting: whereas 0/90 material presents higher K_{mat} (4.47 MPam$^{1/2}$ vs. 4.05 MPam$^{1/2}$), L is significantly lower in 45/−45 material (0.61 mm vs. 2.45 mm in 0/90 material). Consequently, there is a notch radius (ρ^*) beyond which the fracture resistance is higher in 45/−45 material. This is very important in engineering practice because it shows that a material that might seem to be weaker is actually stronger, depending on the kind of notch being analyzed.

Implication 7b is clearly observed in Figure 2.

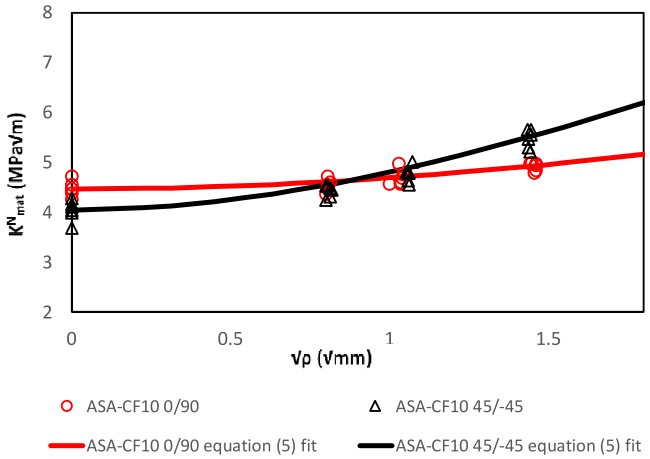

FIGURE 12 | Evolution of apparent fracture toughness (K^N_{mat}) in ASA-CF10 with two different printing raster orientations (0/90, 45–45). [Colour figure can be viewed at wileyonlinelibrary.com]

Another very interesting example may be found in [21, 22], where the authors observed how increasing the grain size of a particular steel (AISI4340) generated a much bigger fracture toughness, but also a bigger L (given that in polycrystalline materials L is approximately proportional to grain size), giving almost a flat line for the notch effect.

2.8 | Reasoning 8

Failure Assessment Diagrams (FADs) are one of the main tools when performing structural integrity evaluations of components containing crack-like defects. A FAD assessment represents the cracked component being evaluated by a point of coordinates K_r (fracture ratio) and L_r (plastic collapse ratio), which evaluate (simultaneously) fracture and plastic collapse conditions and follow Equations (21) and (22):

$$K_r = \frac{K_I}{K_{mat}} \tag{21}$$

$$L_r = \frac{P}{P_L} = \frac{\sigma_{ref}}{\sigma_y} \tag{22}$$

P_L being the plastic collapse load, σ_{ref} being the reference stress and σ_y being the yield strength. The location of the assessment point regarding the Failure Assessment Line (FAL) determines if the component is operating under safe, critical, or unsafe conditions, as shown in Figure 13.

Additionally, the relationship between K_r and L_r indicates the dominant failure mechanism. Approximately [23], if $K_r/L_r > 1.1$, the process is governed by brittle fracture; if $K_r/L_r < 0.4$, the process is governed by plastic collapse, and for intermediate values, the process is controlled by elastic–plastic fracture (see Figure 13).

Cicero [24, 25] proposed to use FADs also for the evaluation of components containing notches by simply substituting K_{mat} by the corresponding K^N_{mat}. For U-shaped notches, K^N_{mat} may be estimated by Equation (5):

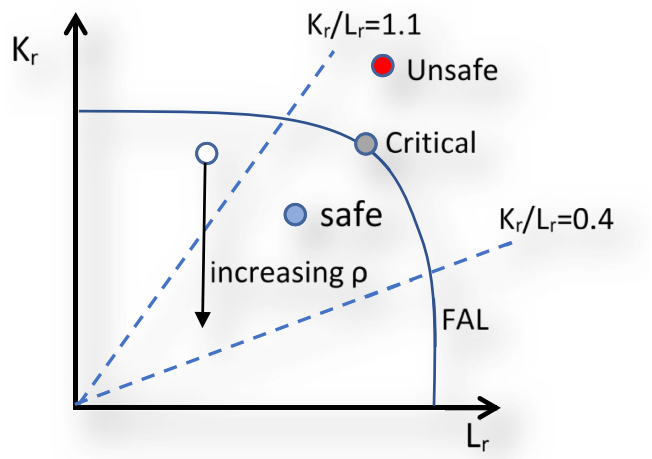

FIGURE 13 | Schematic and fundamentals of FAD assessments. [Colour figure can be viewed at wileyonlinelibrary.com]

14602695, 2026, 7, Downloaded from https://onlinelibrary.wiley.com/doi/10.1111/ffe.70282 by Sheffield Hallam University, Wiley Online Library on [08/06/2026]. See the Terms and Conditions (https://onlinelibrary.wiley.com/terms-and-conditions) on Wiley Online Library for rules of use; OA articles are governed by the applicable Creative Commons License

$$K_r = \frac{K_I}{K_{mat}^N} = \frac{K_I}{K_{mat}\sqrt{1+\frac{\rho}{4L}}} \tag{23}$$

If a component containing a notch is represented in the FAD, the increase in the notch radius implies a vertical displacement (downwards) of the assessment point.

Implication 8. Following the FAD approach, when the notch radius increases, the ratio K_r/L_r decreases, meaning that the failure mechanisms leading to the final fracture may change toward successively more ductile processes. This is in agreement with experimental observations (e.g., [2–4]).

Figure 14 shows an example of the change in micromechanisms in PMMA when the notch radius increases [2]. The fracture surface in basically brittle for notch radius 0.25 mm (critical load 107.1 N), but develops non-linear fracture micromechanisms for notch radius 2.5 mm (critical load 250.4 N). For a given same load level in both specimens, such as the critical load of the first specimen (107.1 N), K_r is 1.11 in the specimen with a notch radius of 0.25 mm, and 0.56 in the specimen with a notch radius of 2.5 mm.

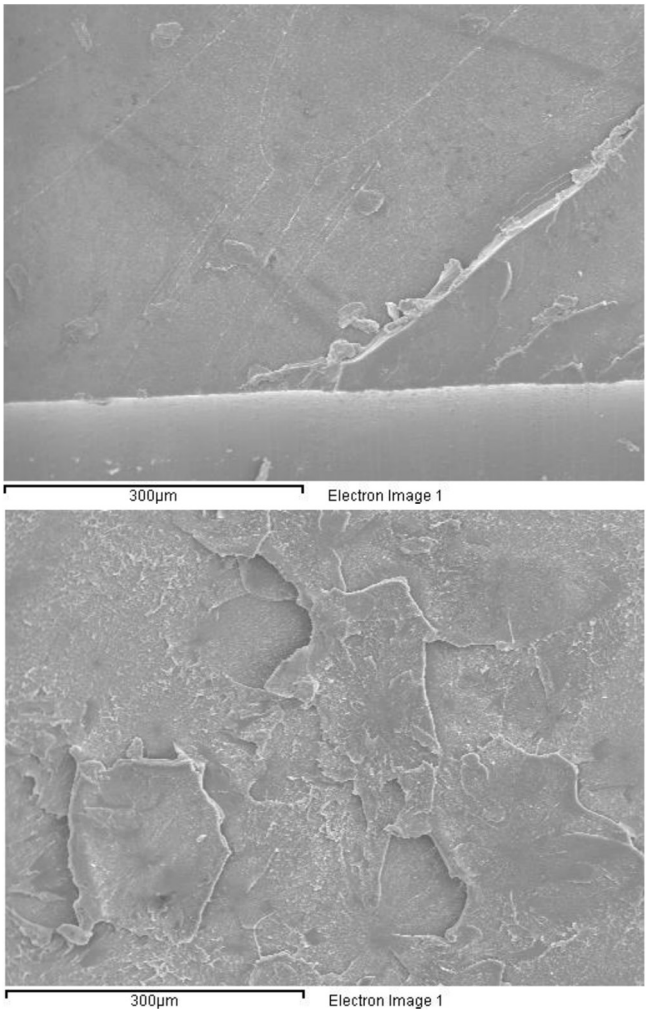

FIGURE 14 | Fracture mechanisms observed in notched specimens. $\rho = 0.25$ mm (top); $\rho = 2.5$ mm (bottom).

3 | Discussion and Conclusions

This paper provides a series of reasonings based on simple formulations derived from the TCD. More precisely, two basic formulas are used: the Point Method failure criterion (Equation (2)), and the apparent fracture toughness prediction derived from the Line Method and the Creager–Paris stress distribution ahead of the notch tip (Equation (5)). These two equations allow different practical implications to be derived, which may be useful when dealing with critical (i.e., fracture) or subcritical cracking processes (e.g., fatigue and stress corrosion cracking). These implications may have usefulness at different stages of the component lifecycle, from the initial design to the final failure analysis, if applicable, as well as its service life.

Essentially, by knowing the ultimate tensile strength (or, more generally, the inherent strength, σ_0), the fracture toughness (K_{mat}), and the corresponding critical distance (L), it is possible to compare the performance of different materials in engineering applications in the presence of any kind of geometrical feature (notch). As an example, if two materials have the same L, the one with the higher inherent stress will withstand a greater critical load.

Finally, beyond this sort of comparisons, two scientific issues with important engineering implications are simply addressed: First, it is shown and justified that, given two materials, one may be superior in cracked conditions or in the presence of sharp notches (the one with higher K_{mat}), while the other can be superior for blunter notches. This is a kind of mistake which a designer might easily make, assuming that one material will always be superior to the other; and second, the application of the apparent fracture toughness estimation mentioned above (Equation (5)) to structural integrity assessments using Failure Assessment Diagrams is able to explain how introducing larger notch radii can generate significant changes in the failure micromechanisms.

Nomenclature

K_I	stress intensity factor
K_{mat}	fracture toughness in stress intensity factor units
K^N_{mat}	apparent fracture toughness in stress intensity factor units
L	critical distance
P	applied load
P_{crit}	critical load
P_L	limit load
r	distance to notch tip
ρ	notch radius
σ_0	inherent stress
σ_{ref}	reference stress
σ_u	tensile strength
σ_y	yield strength

Funding

This work was supported by the Ministerio de Ciencia, Innovación y Universidades (PID2021-122324NB-I00).

14602695, 2026, 7, Downloaded from https://onlinelibrary.wiley.com/doi/10.1111/ffe.70282 by Sheffield Hallam University, Wiley Online Library on [08/06/2026]. See the Terms and Conditions (https://onlinelibrary.wiley.com/terms-and-conditions) on Wiley Online Library for rules of use; OA articles are governed by the applicable Creative Commons License

Data Availability Statement

The data that support the findings of this study are available from the corresponding author upon reasonable request.

References

1. D. Taylor, *The Theory of Critical Distances: A New Perspective in Fracture Mechanics* (Elsevier, 2007).

2. S. Cicero, V. Madrazo, and I. A. Carrascal, "Analysis of Notch Effect in PMMA by Using the Theory of Critical Distances," *Engineering Fracture Mechanics* 86 (2012): 56–72.

3. S. Cicero, V. Madrazo, and T. García, "Analysis of Notch Effect in the Apparent Fracture Toughness and the Fracture Micromechanisms of Ferritic–Pearlitic Steels Operating Within Their Lower Shelf," *Engineering Failure Analysis* 36 (2014): 322–342.

4. S. Cicero, V. Madrazo, T. García, J. Cuervo, and E. Ruiz, "On the Notch Effect in Load-Bearing Capacity, Apparent Fracture Toughness and Fracture Mechanisms of PMMA Polymer, Aluminium Alloy Al7075-T651 and Structural Steels S275JR and S355J2," *Engineering Failure Analysis* 29 (2013): 108–121.

5. F. J. Gómez and M. Elices, "Fracture Loads for Ceramic Samples With Rounded Notches," *Engineering Fracture Mechanics* 73 (2006): 880–894.

6. F. Berto and P. Lazzarin, "Recent Developments in Brittle and Quasi-Brittle Failure Assessment of Engineering Materials by Means of Local Approaches," *Materials Science & Engineering R: Reports* 75 (2014): 1–48.

7. M. Allouti, C. Schmitt, and G. Pluvinage, "Assessment of a Gouge and Dent Defect in a Pipeline by a Combined Criterion," *Engineering Failure Analysis* 36 (2014): 1–13.

8. C. T. Ng and L. Susmel, "Notch Static Strength of Additively Manufactured Acrylonitrile Butadiene Styrene (ABS)," *Additive Manufacturing* 34 (2020): 101212.

9. G. C. Sih, "Strain-Energy-Density Factor Applied to Mixed-Mode Crack Problems," *International Journal of Fracture* 10 (1974): 305–321.

10. G. Pluvinage, "Fatigue and Fracture Emanating From a Notch: The Use of the Notch Stress Intensity Factor," *Nuclear Engineering and Design* 185 (1998): 173–184.

11. P. Lazzarin and R. Zambardi, "A Finite-Volume-Energy-Based Approach to Predict the Static and Fatigue Behaviour of Components With Sharp V-Shaped Notches," *International Journal of Fracture* 112 (2001): 275–298.

12. P. González, S. Cicero, B. Arroyo, and J. A. Álvarez, "A Theory of Critical Distances-Based Methodology for the Analysis of Environmentally Assisted Cracking in Steels," *Engineering Fracture Mechanics* 214 (2019): 134–148.

13. M. Creager and P. C. Paris, "Elastic Field Equations for Blunt Cracks With Reference to Stress Corrosion Cracking," *International Journal of Fracture* 3 (1967): 247–252.

14. S. Cicero, V. Martínez-Mata, L. Castañón-Jano, A. Alonso-Estébanez, and B. Arroyo, "Analysis of Notch Effect in the Fracture Behaviour of Additively Manufactured PLA and Graphene-Reinforced PLA," *Theoretical and Applied Fracture Mechanics* 114 (2021): 103032.

15. S. Cicero, M. Sánchez, V. Martínez-Mata, S. Arrieta, and B. Arroyo, "Structural Integrity Assessment of Additively Manufactured ABS, PLA and Graphene-Reinforced PLA Notched Specimens Combining Failure Assessment Diagrams and the Theory of Critical Distances," *Theoretical and Applied Fracture Mechanics* 121 (2022): 103535.

16. S. Cicero, V. Martínez-Mata, A. Alonso-Estébanez, L. Castañón-Jano, and B. Arroyo, "Analysis of Notch Effect in 3D-Printed ABS Fracture Specimens Containing U-Notches," *Materials* 13 (2020): 4716.

17. V. Madrazo, S. Cicero, and T. García, "Assessment of Notched Structural Steel Components Using Failure Assessment Diagrams and the Theory of Critical Distances," *Engineering Failure Analysis* 36 (2014): 104–120.

18. F. T. Ibáñez-Gutiérrez, S. Cicero, I. A. Carrascal, and I. Procopio, "Effect of Fibre Content and Notch Radius on the Fracture Behaviour of Short Glass Fibre Reinforced Polyamide 6: An Approach From the Theory of Critical Distances," *Composites Part B, Engineering* 94 (2016): 299–311.

19. S. Cicero, T. García, J. Castro, V. Madrazo, and D. Andrés, "Analysis of Notch Effect on the Fracture Behaviour of Granite and Limestone: An Approach From the Theory of Critical Distances," *Engineering Geology* 177 (2014): 1–9.

20. S. Cicero, S. Arrieta, F. Devito, B. Arroyo, and F. Lavecchia, "Fracture Behaviour of Additively Manufactured Carbon Fibre Reinforced Acrylonitrile–Styrene–Acrylate Containing Cracks and Notches," *Journal Of Composites Science* 9 (2025): 185.

21. R. O. Ritchie, B. Francis, and W. L. Server, "Evaluation of Toughness in AISI 4340 Steel Austenitised at Low and High Temperatures," *Metallurgical Transactions A* 7 (1976): 831–838.

22. R. O. Ritchie and R. M. Horn, "Further Considerations on the Inconsistency in Toughness Evaluation of AISI 4340 Steel Austenitised at Increasing Temperatures," *Metallurgical Transactions A* 9 (1978): 331–339.

23. M. Koçak, S. Webster, J. J. Janosch, R. A. Ainsworth, and R. Koers, eds. *FITNET Fitness-for-Service (FFS) Procedure*, vol. 1 (GKSS, 2008).

24. S. Cicero, V. Madrazo, I. A. Carrascal, and R. Cicero, "Assessment of Notched Structural Components Using Failure Assessment Diagrams and the Theory of Critical Distances," *Engineering Fracture Mechanics* 78 (2011): 2809–2825.

25. S. Cicero, "Assessment of Structural Materials Containing Notch-Type Defects: A Comprehensive Validation of the FAD–TCD Methodology on Metallic and Non-Metallic Materials," *Theoretical and Applied Fracture Mechanics* 133 (2024): 104612.

14602695, 2026, 7, Downloaded from https://onlinelibrary.wiley.com/doi/10.1111/ffe.70282 by Sheffield Hallam University, Wiley Online Library on [08/06/2026]. See the Terms and Conditions (https://onlinelibrary.wiley.com/terms-and-conditions) on Wiley Online Library for rules of use; OA articles are governed by the applicable Creative Commons License